Structure and diffusion of intrinsic defects, adsorbed hydrogen, and water molecules at the surface of alkali-earth fluorides calculated using density functional theory

A. S. Foster,[1,2] T. Trevethan,[3,4] and A. L. Shluger[3,4]

[1]*Laboratory of Physics, Helsinki University of Technology, P.O. Box 1100, 02015 Helsinki, Finland*
[2]*Department of Physics, Tampere University of Technology, P.O. Box 692, 33101 Tampere, Finland*
[3]*Department of Physics and Astronomy, University College London, Gower Street, London WC1E 6BT, United Kingdom*
[4]*WPI-AIMR Tohoku University, 2-1-1 Katahira, Aoba, Sendai 980-8577, Japan*

Using periodic density functional theory, we calculate the structure and migration energies of fluorine vacancies and interstitials in the bulk and at the stoichiometric bulk-truncated surface of three alkali-earth fluorides: CaF_2, SrF_2, and BaF_2. We then study the adsorption of water and hydrogen, in both molecular and dissociated form, at the ideal surface, and at neutral and charged vacancies in the surface and subsurface layers. The results demonstrate that in nearly all cases molecular adsorption is strongly favored. For the most probable configurations on the surfaces, we also studied the migration paths and barriers, and found that water is highly mobile on the surface, even when adsorbed at defects. In general, CaF_2 and SrF_2 show similar behavior with respect to water, while adsorption energies and migration barriers for BaF_2 are smaller. Finally, we discuss our results in the context of recent experimental Atomic Force Microscopy studies on CaF_2 and compare to calculations on other insulating surfaces.

I. INTRODUCTION

The interaction of water with inorganic surfaces remains a key research topic, as no matter what the application, the presence of water cannot be avoided. This is increasingly, and obviously, important in studies of biocompatible substrates in liquid,[1] but is also is particularly highlighted in the recent demonstrations of the influence of trace elements of water on surface properties even in ultrahigh vacuum (UHV) conditions.[2] For alkali-earth surfaces, their interaction with water is particularly relevant due to their historical role in acid production[3,4] and their developing role as dielectric thin films in micro- and optoelectronics.[5,6] The basic fluorite bulk and surface structures have been the subject of numerous experimental and computational studies,[7–19] and more recent low-energy electron diffraction studies have looked into the surface's structure in detail.[20] Studies of water on the surface have been more sparse, generally predicting that water weakly interacts with the surface in normal conditions,[21] but can dissociate or even etch the surface in the presence of surface defects or at high pH.[22–25]

The development of atomic force microscopy (AFM), and its capability to study insulating surfaces in atomic resolution[26–29] offers a powerful tool for studying surface properties, and this has also been applied to investigate the surfaces of alkali-earth fluorides. Comprehensive experimental and simulated AFM studies of the CaF_2 (111) surface confirmed the expected surface structure, the F-Ca-F stoichiometric termination, and provided a detailed understanding of the imaging mechanism.[30–33] However, studies of defects on the surface remain difficult to interpret unambiguously.[34–36] In particular, the interaction of water with the CaF_2 (111) surface has been studied via AFM manipulation, and clear evidence for differences in adsorbate mobility were observed, but identification of the adsorbates has not yet been achieved.[37] In all studies of the interaction

of water with the CaF_2 (111) surface, there was no evidence of any reconstructions or global changes in termination.[22–25] In particular, the high resolution AFM studies of water deposition[37] took snapshots of the surface as a function of time during deposition and the contrast pattern of the surface in images remained entirely consistent with earlier studies of the clean surface regardless of the water density.[30–33] Hence, we assume that the situation will be the same for all three materials and consider only the F-M-F stoichiometric termination.

In this work, we use first-principles simulations to characterize the ideal and defective (111) surfaces of three alkali-earth fluorides (MF_2), CaF_2, SrF_2, and BaF_2. Here we define the ideal surface as the stoichiometric bulk-truncated unreconstructed surface, which undergoes only minor atomic displacements from the bulk termination. We concentrate on CaF_2 as our benchmark material, but contrast with BaF_2 and SrF_2 where we observed clear differences in behavior. We further study the adsorption of hydrogen and water on these surfaces, and consider the most likely reaction paths according to relative energetics. In order to provide an indirect link to processes at finite temperatures, we also consider the diffusion and reaction barriers for several defect and adsorbate complexes. Finally, we put our results in the context of previous experimental and computational studies. Note that, in general, we will discuss the properties of all three surfaces simultaneously, and only highlight those areas where substantive differences arise.

II. METHODS

The calculations have been performed using the periodic plane-wave basis VASP (Refs. 38 and 39) code, implementing the spin-polarized density functional theory (DFT) and the generalized gradient approximation.[40] We have used projected augmented wave (PAW) potentials[41,42] to describe the

TABLE I. Comparison of calculated and experimental (in parentheses) structural properties of the MF$_2$ bulk and surface. Here a is the lattice constant, and ΔF^1, ΔM, and ΔF^2 are the displacements in the surface normal direction from the ideal termination of the surface fluorine, metal and subsurface fluorine atomic sublayers, respectively [see Fig. 2(a)].

	CaF$_2$	SrF$_2$	BaF$_2$
a(Å)	5.50 (5.42[a])	5.85 (5.80[a])	6.30 (6.20[a])
ΔF^1(Å)	0.01 (−0.03[b])	−0.02	−0.09 (−0.12[b])
ΔM(Å)	0.01 (−0.01[b])	0.00	−0.01 (−0.01[b])
ΔF^2(Å)	−0.02 (−0.01[b])	−0.01	−0.03 (0.01[b])

[a]Reference 13.
[b]Reference 20.

core electrons. The potential for F was generated in the electron configuration [$1s^2$]$2s^22p^5$, Ca in [Ne $3s^2$]$3p^64s^24d^{0.01}$, Sr in [Ar $3d^{10}$]$4s^24p^65s^2$, Ba in [Kr $4d^{10}$]$5s^25p^66s^2$, O in [$1s^2$]$2s^22p^4$, and H in $1s^1$, with the core electrons given in square brackets. A kinetic energy cutoff of 500 eV and a k-point Monkhorst-Pack grid[43] of $5\times5\times5$ per MF$_2$ unit (Γ point for slab calculations) was found to converge the total energy of our systems to within meV. This setup reproduced the experimental bulk structural properties of CaF$_2$, SrF$_2$, and BaF$_2$ to within 2% (see Table I). The calculated bulk band gaps were 8.0, 5.9, and 6.2 eV for CaF$_2$, SrF$_2$, and BaF$_2$, respectively—lower than the experimental values of 12.1, 11.3, and 11.0 eV,[44] as expected for DFT calculations.[45]

For bulk calculations we used a $2\times2\times2$ supercell in terms of the 12 atom conventional cubic fluorite (structure space group: *Fm*-3*m*) unit cell. For surface calculations we checked the dependence of surface relaxations on both slab and vacuum depth, and found them well converged for a slab three layers deep with a vacuum of 1.7 nm. The relaxations of the surface atoms were in good agreement with recent experimental results (see Table I). In order to avoid artificial interactions between molecules on the surface we used a large 2×2 surface unit cell ensuring that defects and molecules are separated by over 1.5 nm from their images. All migration barrier calculations were made using the Climbing Image Nudged Elastic Band method,[46] starting from a small number of images and increasing them until a convergent path was found (for simple paths one image can be enough, but generally we found three or five images was sufficient).

Formation (E_F) energies of defects in the bulk and surface were calculated as follows:

$$E_F^q = E_D^q - (E_{atom}^q + E_{ref}),$$

where E_D^q is the energy of the defective system in charge state q, E_{atom}^q is the isolated neutral or charged atom being considered, i.e., an F atom for neutral interstitials and vacancies, and an F$^-$ ion for charged interstitials and vacancies, and E_{ref} is the defect-free reference bulk or surface system equivalent in size to E_D^q. Adsorption (E_A) energies on the surface were calculated as follows:

$$E_A^q = E_D^q - (E_{spec} + E_{surf})^q,$$

where E_D^q is the energy of the adsorbed system in charge state q, E_{spec} is the isolated neutral or charged atom/molecule being considered and E_{surf} is the reference surface system (which can be defected) equivalent in size to E_D^q. Atom numbers and charge are always conserved on either side of the equality. This choice assumes a specific electron chemical potential and that the dissociation energy of F$_2$ has been paid already—other choices just result in a uniform shift in values and would not affect our conclusions. For comparisons between charged and neutral systems, and calculations of ionization potentials and electron affinities we align energy levels with respect to the vacuum level, defined as the position in the vacuum where the mean electrostatic potential converges.[47] The calculated electron affinity of a fluorine atom is 3.3 eV, in good agreement with the experimental value of 3.4 eV.[48]

We also corrected for artificial electrostatic interactions in the periodic system where present by calculating monopole and dipole corrections explicitly, and scaling them according to the dielectric constant of the environment (CaF$_2$ 6.76, SrF$_2$ 7.69, and BaF$_2$ 7.33).[49,50] Since CaF$_2$ has both the smallest lattice and dielectric constant, the error introduced by artificial electrostatic interactions for the same unit cell size is certainly larger in CaF$_2$, than in SrF$_2$ and BaF$_2$. However, the corrections introduced should reduce this effect, but not completely.[47]

More generally, the DFT approach gives good accuracy for geometries and relative energetics of ground-state systems, and we can expect an overall error on the order of 0.1 eV in our results.[45,47]

III. RESULTS

Before considering their interaction with adsorbates, it is interesting to look directly at the properties of defects in the bulk and the surface, in particular, anion interstitials and vacancies are the most probable surface defect—especially for cleaved surfaces.[13] Since we cannot readily determine the ratio of neutral and charged defects in the surface, they must be considered in parallel. Note that in conventional nomenclature for alkali-earth halides, and many insulators, a neutral vacancy is known as an F center, and an interstitial is known as an H center. However, we will only use these terms in the context of previous studies to avoid confusion with references to fluorine and hydrogen elements.

A. In the bulk

1. Interstitials

Although bulk defects do not directly influence the adsorption of water at the surface, in order to understand possible routes to defect generation at the surface we initially consider the properties of anion interstitials and vacancies in the bulk of CaF$_2$ (cation vacancies and interstitials have much higher formation energies, see, e.g., Ref. 51). Bulk alkali-earth halides have an fcc sublattice of cations with the anions occupying all the tetrahedral sites. Both neutral (F$_i^0$)

TABLE II. Formation and migration energies for anion interstitials and vacancies in bulk CaF_2. Experimental values are given in parentheses if available.

Defect	Formation energy (eV)	Migration energy (eV)
F_i^0	−0.23	0.2
F_i^-	3.24	0.5 (0.8–0.9[b],[c])
V^0	7.90	1.0 (0.7[a])
V^+	−1.13	0.2 (0.5–0.6[b],[c])

[a]Reference 10.
[b]Reference 11.
[c]Reference 13.

and charged (F_i^-) interstitials occupy octahedral sites sitting between four anions and four cations. Around the neutral interstitial site, lattice F^- ions relax by about 0.2 Å away from the interstitial site and lattice Ca^{2+} ions relax about 0.1 Å towards the defect. There is a further 0.1 Å relaxation of cations towards the interstitial F_i^- compared to the neutral interstitial. We also found a configuration equivalent to the H center discussed in the literature,[12,13] where the F_i^0 forms a covalent bond of 2.1 Å with a lattice F^- ion. This configuration is, however, 0.14 eV higher in energy than the octahedral site with the F_i^0 at a distance of about 2.5 Å from surrounding lattice F^- ions. Although both configurations are spin-polarized and have a magnetic moment of $1\mu_B$, the spectra measured in electron spin resonance (ESR) studies of CaF_2 and other halides support the H-center model.[12,52] However, other recent DFT calculations also predict that the neutral interstitial occupies the octahedral site in CaF_2.[51] Since the energy difference between the two states in our calculations is small, it is difficult to make any strong conclusions and the issue requires further investigation with more advanced exchange-correlation functionals.

In both charged and neutral states, the interstitials diffuse by an exchange mechanism (also known as the interstitialcy mechanism).[53] The charged species has a higher barrier due to its increased electrostatic interaction with the surrounding lattice causing larger displacements of atoms during migration (see Table II). Due to the fact that there is no bond between F_i^0 and lattice F^- ions, there is no covalent bond-breaking contribution to the barrier, in contrast to, for example, migration of oxygen in some oxides by the same mechanism.[54]

2. Vacancies

Removing an F atom from the crystal creates a neutral anion vacancy, V^0. This, however, causes very small distortion of the surrounding lattice due to the predominant localization of the electron at the vacancy. Removing an F^- ion creates a V^+ vacancy having a local positive charge with respect to the lattice. This causes a much stronger lattice deformation with displacements of anions towards the vacancy site by about 0.2 Å and similar displacements of cations away from the vacancy. The vacancy diffusion is equivalent to a displacement of one of the nearest neighbor

F^- ions into the vacancy. The presence of the electron at the V^0 site means that this electron and the F^- must exchange places. This requires overcoming a relatively high barrier of about 1 eV (see Table II). On the other hand, the empty V^+ vacancy facilitates migration of F^- ions with a 0.2 eV barrier.

Although the band gap is underestimated (see Sec. II), we can use the location of defect levels relative to the bands as a qualitative measure of their character. The highest occupied state of V_s^0 is at about 7 eV above the valence band maximum, in reasonable agreement with the 7.4 eV obtained in GW studies of bulk CaF_2.[55] This is about 1 eV below the conduction band. Previous studies of F-center type defects in wide band-gap oxides[56] have shown that their states to a good approximation are pinned to the valence band and the underestimation of the band gap can be corrected using a *scissor operator* approach by raising the conduction band. The experimental value of the band gap in CaF_2 is 12.1 eV. Then this will represent a deep state in the bulk.[47] Upon removing this electron, forming V^+, the density of states now shows an unoccupied defect state at about 0.7 eV below the conduction band.

Although the individual formation energies cannot be directly compared to experiment, the Frenkel energy for the formation of the charged or neutral pair of defects can be (the Frenkel energy is the formation energy of a vacancy and interstitial pair with zero net charge, e.g., V^0 and F^0 or V^+ and F^-, and is found by simply summing the formation energy of the two components). Combining the values in Table II gives an energy cost of 7.68 eV to form a neutral interstitial and vacancy, and 2.10 eV for the charged pair. The latter value is in reasonable agreement with the experimental estimate of about 2.7–3.0 eV (Refs. 11 and 13) (found by separating the migration and formation contributions from the experimental activation energy). The calculated diffusion barriers are also in reasonable agreement with existing experimental data for the migration of the Frenkel pair (F_i^- / V^+), especially in terms of the relative barrier heights. Our results for formation energies of V^0, and of the Frenkel pair are also in good agreement with the recent first-principles calculations[51] (note that the reference for the fluorine atom in Ref. 51 is about 0.4 eV higher in energy than our, so their values are shifted up, but otherwise are very similar). For neutral vacancy migration, the authors of Ref. 51 used artificial constraints on the system, therefore we cannot really compare our calculated barriers. We note that our barrier is in reasonable agreement with experimental estimates (see Table I).

In order to gain more insight into the relative distributions of bulk defects in equilibrium we have also explored their formation energy as a function of the chemical potential of the fluorine and electron reservoirs. Figure 1 shows the formation energies of neutral and charged interstitials and vacancies for three different chemical potentials for fluorine. These represent limits from the source being an atomic or molecular fluorine gas, up to the source being bulk CaF_2. In general we see that the conditions where formation of a neutral interstitial is favored over a charged one are very limited [see Fig. 1(a)], while a charged vacancy is favorable for small electron chemical potentials [see Fig. 1(b)].
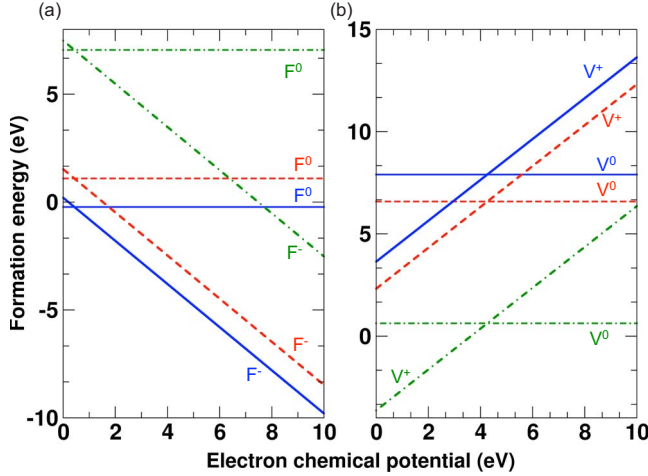
FIG. 1. (Color online) Calculated formation energies as a function of electron chemical potential for (a) bulk interstitials and (b) bulk vacancies. The formation energies for neutral and charged defects are calculated with respect to the reference chemical potential of fluorine, and are plotted as a "pair" in the same color. The reference chemical potentials are as follows: the isolated F atom (blue solid line); fluorine rich, the energy of F in the F_2 molecule (red dashed line); fluorine-poor, the energy of F in bulk CaF_2 (green dot-dashed line).

B. At the surface

1. Interstitials

At the surface, extra F ions or atoms can be stabilized in the subsurface layer or become adatoms. First, we consider neutral, F_s^0, and charged, F_s^-, adatoms. The neutral adatom bonds to a surface F^-, but then gains about 0.3 eV by tilting towards a neighboring Ca^{2+} site [see Fig. 2(c)]. The adatom effectively forms a polarized F_2^- molecule at the surface, which is similar to the classical model of an H center expected in the bulk (see discussion in Sec. III A). This is also characteristic to other halide surfaces, such as NaCl.[57,58] We note that DFT in this case describes relatively well the bonding between the F atom and the surface ion. The charged F_s^- forms an ionic bond with the surface Ca^{2+} ion and adsorbs
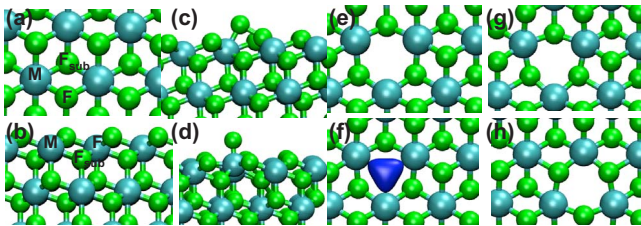

FIG. 2. (Color online) Calculated structures of the ideal (111) surface (a) top view, (b) side view, (c) neutral adatom (F_s^0), (d) charged adatom (F_s^-), (e) a neutral vacancy (V_s^0) including (f) a plot of the spin density isosurface at 0.03 Hartree/Bohr, (g) a charged vacancy (V_s^+), and (h) a subsurface charged vacancy (V_{sub}^+). The structures shown are for CaF_2, but the geometries for the other surfaces are almost identical when scaling for the different lattice constant is taken into account. For clarity, in top views only the upper three atomic layers are shown.

TABLE III. Adsorption and migration energies for neutral and charged F adatoms at the surface of CaF_2.

Defect	Adsorption energy (eV)	Migration energy (eV)
F_s^0	−1.26	0.2
F_s^-	−0.92	0.2

directly above a Ca^{2+} ion in the surface [see Fig. 2(d)]. Both species would be stable on the surface at room temperature. Diffusion of F_s^0 occurs by a slight stretching of the covalent F-F bond (the barrier step), while pivoting around a lattice Ca, then formation of a new F-F bond. For diffusion of F_s^-, the path is almost direct from lattice Ca to lattice Ca, with neighboring lattice fluorines displacing away from the adatom as it diffuses. Both processes are energetically cheap (with both barriers due to small displacements of lattice fluorines) and the adatoms are highly mobile (see Table III).

Neutral interstitial atoms are not stable in the subsurface layer, i.e., interstitial sites near to F_{sub} lattice sites, and relax without a barrier to the surface adatom configuration. However, charged interstitials are stable at subsurface sites due to the increased barrier for migration, and have an equivalent formation energy to F_s^-—they occupy a position almost identical to that of bulk charged interstitials (F_i^-—see Sec. III A 1), with the allowed displacement of surface fluorine ions greatly reducing the formation energy in comparison to the bulk.

2. Vacancies

The atoms around the V_s^0 vacancy at the surface are only slightly displaced from their ideal surface sites [~0.05 Å, compare Figs. 2(a) and 2(e)]. This is because the residual electron is still predominantly localized in the vacancy [F center, see Fig. 2(f)]. In the case of the charged surface vacancy, V_s^+, the relaxation of neighboring atoms is much larger, with M^{2+} ions around the vacancy displacing away by about 0.3 Å, [see Fig. 2(g)], and F^- ions displacing to the vacancy. This is very similar to the relaxations for vacancies in the bulk. The electronic structure of the defects is also very similar to that discussed for bulk, with the relative values shifted due to the smaller band gap of the CaF_2 surface (6.6 eV).

For both types of vacancy the trends in formation energies (see Table IV) are fairly consistent across the different metal

TABLE IV. Formation energies (eV) of surface and subsurface vacancies with respect to removal of a fluorine atom (V^0 and V_s^0) and a F^- ion (V^+ and V_s^+).

System	CaF_2	SrF_2	BaF_2
V_s^0	7.64	7.53	7.38
V_s^+	3.33	3.57	3.32
V_{sub}^0	7.88	7.81	7.66
V_{sub}^+	3.20	3.49	3.31

TABLE V. Calculated vacancy migration barriers (eV).

System	CaF$_2$	SrF$_2$	BaF$_2$
V_s^0	1.3	1.3	1.1
V_s^+	1.0	0.9	0.8
$V_{sub}^0 \Rightarrow V_s^0$	0.4		
$V_s^0 \Rightarrow V_{sub}^0$	0.6		
$V_{sub}^+ \Rightarrow V_s^+$	0.2		
$V_s^+ \Rightarrow V_{sub}^+$	0.1		

cations, and are generally lower than those for similar defects in the bulk.[59] For the neutral vacancies the formation energy reduces with increasing metal ionic radii and lattice constant, with BaF$_2$ having the smallest energy for both V_s^0 and V_{sub}^0. For the charged vacancies, the formation energy scales with the ionicity of the crystal and the lattice constant—SrF$_2$ strikes a balance between these factors, having intermediate ionicity and lattice constant, and has a slightly higher formation energy for charged vacancies as a consequence.

Since the third layer fluorine sublattice is also accessible to adsorbates [see Figs. 2(a) and 4(h)] we also calculated the properties of subsurface vacancies in this layer. In general these defects showed similar trends in relaxations and electronic structure to the surface vacancies. Table IV shows that for V^0 the subsurface site (V_{sub}^0) was unfavorable in all surfaces, but for V^+ the subsurface vacancy (V_{sub}^+) was slightly lower in energy than the surface vacancy for CaF$_2$ and degenerate for BaF$_2$. The favoring of subsurface vacancy sites is also predicted for the (111) surface of another fcc ionic crystal, ceria (CeO$_2$).[60]

The barriers for surface vacancy migration (see Table V) are strongly dependent on the path considered. Within the uppermost atomic fluorine layer, both vacancies diffuse by a lattice F$^-$ ion pivoting around an ionic bond to a neighboring Ca^{2+} ion. This effectively breaks two existing ionic bonds (see Fig. 2) and requires overcoming a barrier of at least 1 eV. The barriers for V_s^0 diffusion by this mechanism were consistently higher by about 0.3 eV than for V_s^+, while the barriers for diffusion on the BaF$_2$ surface were smaller than the other two surfaces. However, surface vacancies can also diffuse by exchanging with subsurface sites—in this case the lattice F$^-$ ion can pivot around two of its existing ionic bonds to lattice Ca^{2+} ions, breaking only one. In general this reduces the barrier significantly (see Table V), and both vacancies will migrate via the subsurface-surface path. V_s^+ will be highly mobile, as in the bulk, but the presence of the residual electron in V_s^0 increases its barrier, and it will be relatively stable in the surface site.

C. Water adsorption

1. At the ideal surface

On the ideal surfaces, water adsorbs on top of the metal site with a slight tilt due to hydrogen bonding with a neighboring fluorine [see Fig. 3(a)]. Since there are three symmetric fluorine ions around each cation, the water molecule can effectively occupy three equivalent configurations. In Fig. 3
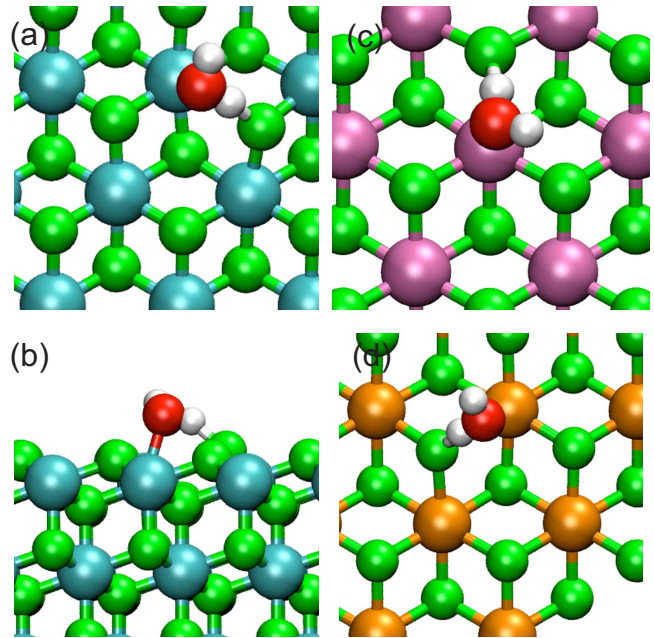

FIG. 3. (Color online) Calculated structures for water adsorbed on the ideal surfaces of (a) CaF$_2$ top view, (b) CaF$_2$ side view, (c) SrF$_2$, and (d) BaF$_2$.

the three possible configurations are shown, one on each of the surfaces considered, but they are effectively equivalent with a barrier of only about 0.1 eV to move between them. At room temperature, previous calculations of water on the CeO$_2$ (111) surface suggest that the molecule is likely to rotate continuously through all three configurations.[61,62] Despite being relatively weak adsorption, this associated adsorption is overwhelmingly favored, in agreement with previous experimental studies on CaF$_2$ (111) and BaF$_2$ (111),[23] and theoretical studies on CaF$_2$ (111).[21] In particular, by comparing the energies of the molecularly adsorbed H$_2$O with that of the dissociated (OH+H), we see that dissociation costs over 3 eV in energy (see Table VI). We have also considered the situation where water is already dissociated on the surface, and calculated an OH group at a metal site and a H on a neighboring fluorine site on the surface. We found that the OH and H will spontaneously recombine to reform a water molecule without barrier.

Calculations of the diffusion barrier (see Table VII) show that water will be highly mobile on all the surfaces at room temperature with barriers of a few tenths of an eV. This can be compared to the TiO$_2$ (110) surface, where the diffusion barrier for molecular water is around 0.2 eV and it is known to be mobile at room temperature.[63] The water molecule has initially two bonds, Ca-O (2.43 Å) and H-F (1.63 Å), as shown in Fig. 4(b). During diffusion, it first rotates to form a new H-F bond (2.60 Å) in the direction of diffusion [costing about 0.1 eV, see Fig. 4(c)], with the Ca-O bond remaining almost the same (2.47 Å). The molecule then effectively pivots around this bond, increasing the Ca-O distance [2.84 Å in Fig. 4(d) and 3.67 Å in Fig. 4(e)] and reducing the H-F distance [2.32 Å in Fig. 4(d) and 1.84 Å in Fig. 4(e)]. This allows it to cross to a neighboring cation forming a new Ca-O bond [2.80 Å in Fig. 4(f)] and reach the equilibrium H-F distance [1.65 Å in Fig. 4(f)].

TABLE VI. Adsorption energies (eV) for water at ideal and defected surfaces. Reference (H_2O) is for associated molecular adsorption, while values for (OH+H) refer to the dissociated state, and (O+H+H) includes also dissociation of OH. For all energies E_{spec} is for the isolated H_2O molecule and E_{surf} is either the ideal or defective surface being considered.

System	Reference	CaF_2	SrF_2	BaF_2
Ideal	H_2O	−0.51	−0.47	−0.49
Ideal	OH+H	2.80	3.00	2.78
V_s^0	H_2O	−0.70	−0.65	−0.61
V_s^0	OH+H	−0.54	−0.33	−0.11
V_s^0	O+H+H	+2.76		
V_s^+	H_2O	−0.70	−0.66	−0.55
V_s^+	OH+H	0.36	0.45	0.58
V_s^+	O+H+H	+5.67		
V_{sub}^+	H_2O	−0.49		−0.47
V_{sub}^+	OH+H	4.89		4.79

2. At vacancies

At V_s^0 defects on the surfaces, water adsorbs just at the side of the vacancy, bonding to two metal ions [see Fig. 5(a)] and gaining about 0.2 eV more than when adsorbing on the ideal surfaces (see Table VI). Simulating the dissociative adsorption, we find that the hydroxyl group binds to the three metal cations surrounding the vacancy [see Fig. 5(b)] in the OH⁻ state. It is effectively picking up a residual electron from the vacancy to stabilize in its favored OH⁻ state. The second hydrogen therefore remains a neutral atom; it does not bind to the surface, and can leave without energy cost. Although in general the dissociative adsorption is less favored than molecular adsorption, the energy differences are much smaller than for the ideal surface. In particular, the dissociated state is only 0.16 eV higher in energy than the molecular state on CaF_2 (see Table VI). Furthermore, there are some significant differences in the energies of adsorption at the neutral vacancy between CaF_2 and BaF_2. Molecular adsorption results in a similar gain in energy, but dissociation is clearly more energetically favored on CaF_2 than on BaF_2—the dissociated state is 0.50 eV higher in energy on

TABLE VII. Migration energies (eV) for water at ideal and defected surfaces. Reference (H_2O) is for associated molecular adsorption, while values for (OH+H) refer to the dissociated state.

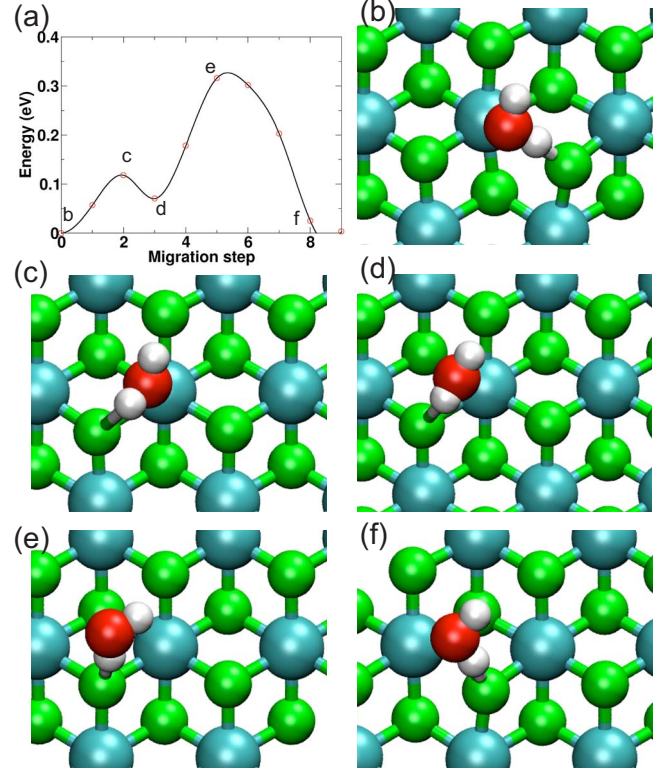| System	Reference	Diffusing Species	CaF_2	SrF_2	BaF_2
Ideal	H_2O	H_2O	0.3	0.3	0.2
V_s^0	H_2O	H_2O	0.4		
V_s^0	H_2O	V_s^0+H_2O	1.2	1.3	0.9
V_s^0	OH+H	OH	2.2		
V_s^0	OH+H	OH+V_s^0	2.1		
V_s^+	H_2O	H_2O	0.3		
V_s^+	H_2O	H_2O+V_s^+	0.9	0.9	0.7
V_{sub}^+	H_2O	H_2O+V_{sub}^+	0.1		

FIG. 4. (Color online) (a) Barrier for a water molecule diffusing on the ideal CaF_2 (111) surface, and (b)–(f) snapshots of the diffusion path at points labeled in the barrier plot.

BaF_2. This is mainly due to the larger lattice constant of BaF_2, which results in longer bonds [compare Figs. 5(b) and 5(e)], and a general reduction in adsorption energies and migration barriers. As one would expect, SrF_2 lies between the two, with a 0.32 eV difference. We also considered dissociation of water leaving hydrogen in the vacancy, and a hydroxyl on the surface, but this was energetically very unfavorable.

In order to look in more detail at the dissociation mechanism of water at V_s^0 and to assess our accuracy, we can split the reaction processes into several stages and compare the calculated energy costs to available experimental data (see Table VIII). The steps we consider are as follows: the initial state is molecular water in the gas phase and a V_s^0 on the surface (I). Water can then dissociate in the gas phase (II) at a cost of over 5 eV. Ionizing the vacancy to free an electron (III) costs a further 2.6 eV, but then 1.7 eV is gained by localizing the electron on the OH (IV). The OH⁻ then gains almost 7 eV by adsorbing on the positive vacancy in the surface (V) and the remaining hydrogen atom gains zero energy by adsorbing to the surface (VI). This shows that where comparison to experiment is possible, our calculated values are within a few percent and are capturing the energetic costs of the key components in the reaction. However, the obtained accuracy is certainly not high enough to unambiguously decide the state of water adsorbed at V_s^0 sites, and the calculations effectively predict that initially both molecular and dissociated water could be present. We also simulated the dissociation reaction at V_s^0 explicitly, and found that the bar-
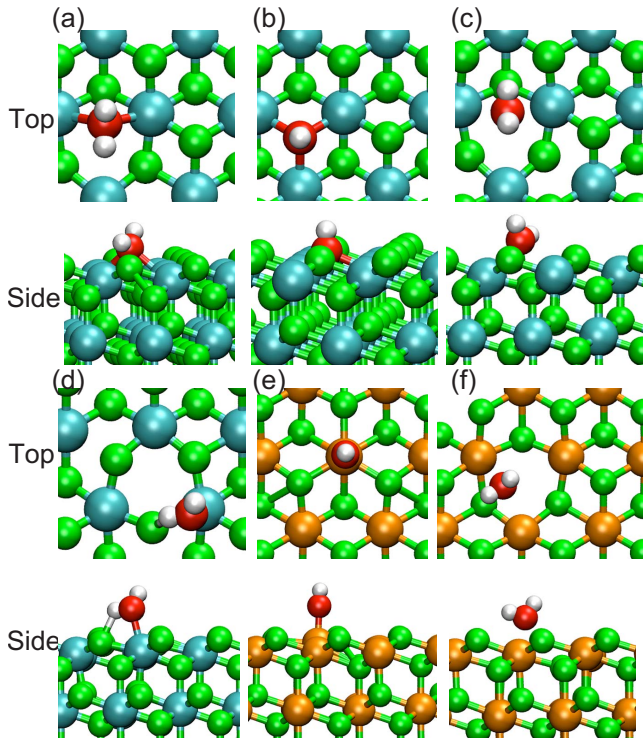
FIG. 5. (Color online) Calculated structures for water adsorbed on the CaF$_2$ surface (a) molecularly adsorbed at a V_s^0, (b) dissociated at a V_s^0, (c) molecularly adsorbed at a V_s^+, (d) molecularly adsorbed at a V_{sub}^+, and on the BaF$_2$ surface, (e) dissociated at the ideal surface V_s^0, and (f) molecularly adsorbed at a V_s^+.

rier for dissociating a water molecule adsorbed at the neutral vacancy is only 0.46 eV.

The geometry of water adsorption at the charged V_s^+ vacancy is almost identical to the neutral case [see Fig. 5(c)], with the main differences obviously resulting from the absence of an extra electron at the vacancy site. This results in an increase in attraction to the locally charged site compared to the neutral case, but this is compensated by the increased bond length to the adsorbate due to relaxation of the metal cations away from the vacancy. The adsorption energies are of a similar magnitude to V_s^0 (see Table VI). For all surfaces,

TABLE VIII. Breakdown of calculated reaction processes during dissociation of water at a neutral vacancy, V_s^0, in the CaF$_2$ surface. All values are in eV and experimental values are given in parentheses.

Step	Reaction	Energy (eV)
I	H$_2$O(gas)$+V_s^0$	0.0
II	H^0(gas)$+$OH^0(gas)$+V_s^0$	$+5.36(+5.10)$[a]
III	H^0(gas)$+$OH^0(gas)$+V_s^+$+e$^-$	$+2.60$
IV	H^0(gas)$+$OH$^-$(gas)$+V_s^+$	$-1.71(-1.8)$[b]
V	H^0(gas)$+V_s^+$OH$^-$	-6.79
VI	H^0$+V_s^+$OH$^-$	0.0

[a]Ref. 64.
[b]Refs. 65–67.

molecular adsorption is strongly favored by over 1 eV.

Although unlikely to exist, it is interesting to compare the dissociated state of water at V_s^+ with that at V_s^0. Now that there is no electron localized in the vacancy, the hydrogen atom is ionized and the proton adsorbs to the surface. This is strongly bound, and it is energetically preferable to etch an HF molecule from the surface (+0.39 eV with reference to the surface with an adsorbed hydroxyl group) rather than the proton (+4.16 eV). This etching of the surface by water has been observed to occur for more basic conditions and to dominate surface chemistry above pH 11 (Ref. 25)—conditions where there would be a prevalence of available OH species.

At the subsurface V_{sub}^+ site, the presence of the vacancy does little to change the molecular adsorption energy from the ideal surface case, and the geometry of adsorbed state is very similar [see Fig. 5(d)]. However, due to the lack of available space above the vacancy, the dissociated water state is much more unfavorable. We also considered the further dissociation of an adsorbed hydroxyl, leaving only oxygen at the vacancy and two hydrogens on the surface—this proved to be energetically unfavorable for both kinds of vacancy (see Table VI).

Unsurprisingly, the relatively small increase in molecular adsorption energies at these defects means that the migration barriers for adsorbed molecule are also quite similar to those for the ideal surface. On the CaF$_2$ surface, the barrier to dissociate a water molecule from a V_s^0 is about 0.4 eV, only 0.1 eV higher than that for diffusion on the ideal surface (see Table VII). At a V_s^+ site there is basically no interaction and the barrier is the same as on the ideal surface. In contrast, for dissociated water, the hydroxyl species is strongly bound at the V_s^0 site, with a migration barrier of 2.2 eV.

In order to explore whether water can play a role in changing the mobility of intrinsic defects in the surface, we also calculated the barriers for diffusion of the adsorbate-vacancy complex. Table VII shows that in all cases the barrier for the combined diffusion of vacancy and water molecules is similar (or a little smaller) to the barrier for diffusion of the vacancy in the uppermost surface alone, around 1 eV. This can also be seen in the diffusion path in Fig. 6, where the initial steps show the diffusion of the F towards the vacant site, while H$_2$O bonds to a lattice Ca. Once the F crosses the saddle point, H$_2$O diffuses to the new vacancy site. The higher barrier of the separate diffusion process also dominates in the combined diffusion of V_s^0 and OH [see Fig. 4(d)], costing just 0.1 eV less than diffusion of the OH group out of the vacancy. The generally low cost of diffusion of the subsurface vacancy is reflected in the diffusion of the (H$_2$O$+V_{sub}^+$) complex. Here, V_{sub}^+ diffuses to the surface, forming V_s^+, and the water molecule moves to sit on top of a surface Ca site (its ground state on the ideal surface). This costs about 0.1 eV, and a similar diffusion process and cost to a neighboring subsurface site facilitates the migration. Here, water is reducing the barrier for vacancy migration to the surface (from 0.2 to 0.1 eV)

3. Hydrogen adsorption

As part of the reaction of water with the surface we have already considered the interaction of hydrogen atoms and
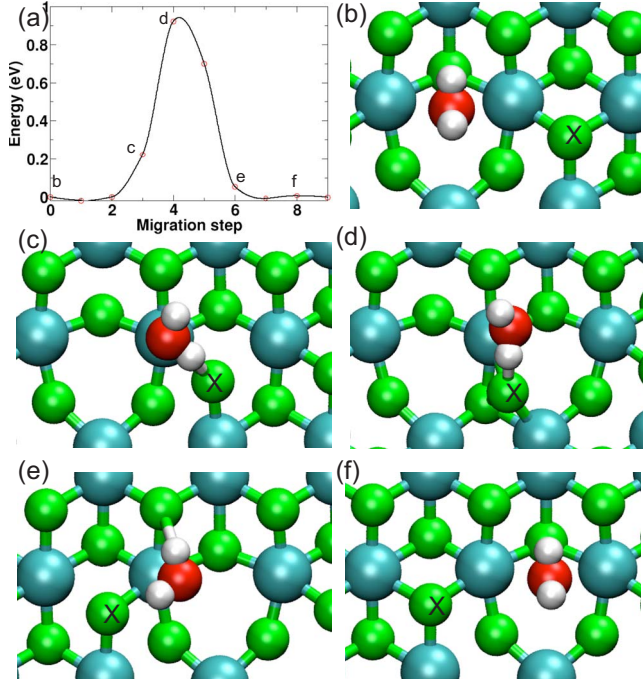
FIG. 6. (Color online) (a) Barrier for a water molecule adsorbed at a V_s^+ site diffusing on the CaF$_2$ (111) surface, and (b)–(f) snapshots of the diffusion path at points labeled in the barrier plot. The diffusing fluorine ion is labeled by "X."

protons with the ideal surface, but hydrogen can generally be present as an environmental impurity or as a consequence of dissociation and may itself react with a vacancy. Table IX shows that a hydrogen atom will adsorb strongly at a V_s^0 site in the surface, gaining over 3 eV and sitting almost in-plane with the surrounding Ca^{2+} ions. In contrast, as on the ideal surface, the absence of an extra electron at the V_s^+ site means that hydrogen gains very little energy by adsorbing there. Note that the interaction of a hydrogen atom with the V_s^+ is equivalent to a proton adsorbing at a V_s^0 site (we did not consider the adsorption of a proton at a V_s^+ site due to the strong electrostatic repulsion).

Similarly, H$_2$ does not adsorb at the V_s^+ site. At V_s^0 it actually *bonds* to a neighboring Ca, but the adsorption energy

TABLE IX. Adsorption energies of hydrogen at vacancies in the CaF$_2$ surface. Reference (H) is for atomic adsorption, (H+H) dissociative molecular adsorption and (H$_2$) associated molecular adsorption. For H adsorption E_{spec} is for the isolated H atom, and for H$_2$ and (H+H) adsorption E_{spec} is for the isolated H$_2$ molecule. For all energies E_{surf} is either the ideal or defective surface being considered.

System	Reference	Adsorption energy (eV)
V_s^0	H	−3.47
V_s^0	H+H	+1.02
V_s^0	H$_2$	−0.06
V_s^+	H	−0.04
V_s^+	H+H	+4.45
V_s^+	H$_2$	−0.08

TABLE X. Adsorption energies at etched defect complexes. In type adsorption (i) the adsorbant displaces a surface fluorine ion directly down into a subsurface interstitial position; and in type (ii) the adsorbant displaces a surface fluorine ion into an adatom position on the surface.

System	Type	Adsorption energy (eV)
V_s^0+H	(i)	−1.59
OH+H	(i)	+2.39
OH+H	(ii)	+0.04

is tiny. If we consider the hydrogen molecule dissociation at vacancies, then the fairly large dissociation energy of the molecule, calculated as 4.50 eV (experimental value 4.52 eV),[48] must be compensated by adsorption of one hydrogen at the vacancy and one on the surface. This means that dissociation at the V_s^+ site is strongly energetically unfavorable, since no energy is gained by adsorption of either isolated hydrogen. Even at the more reactive V_s^0 site, the gain due to adsorption of hydrogen atom at the vacancy is not enough to compensate the dissociation energy, and molecular adsorption is favored by over 1 eV.

Unlike water and its reaction products, the very weak bonding of hydrogen atom to the ideal surface means that it only loses energy when it moves out from the defect site, regaining nothing from adsorption to the surface. Therefore separating hydrogen atom from the neutral vacancy is very expensive, with the barrier to remove hydrogen from the V_s^0 site being at least 3.5 eV. Diffusion of the whole hydrogen-vacancy complex costs more than 5 eV.

4. Surface atom displacement

As mentioned in Sec. III C 2, there exists experimental evidence for weak etching of the surface in the presence of water, i.e., the process of surface material removal by water. Although we do not attempt to model this process directly, we have considered several cases where the adsorbing species displaces a surface lattice ion to form the defect complex as an initial stage of etching process. Specifically, we consider the creation of an anion vacancy/interstitial pair due to the hydrogen atom and water molecule adsorption process. Our calculations exposed two mechanisms that provided additional reaction routes for adsorbates with the surface: (i) the adsorbant displaces a surface fluorine ion directly down into a subsurface interstitial position; (ii) the adsorbant displaces a surface fluorine ion into an adatom position on the surface. In both cases, the adsorbant exposes a vacancy and immediately gains in adsorption energy, but the gain must be larger than the cost of the displacement of fluorine ion. We explored this for all the key adsorption cases discussed in the previous sections, and significant examples are listed in Table X.

The first example is hydrogen adsorbing near to a V_s^0 site. We note that the energetically favorable state, as discussed in Sec. III C 3, is for hydrogen to adsorb in the vacancy, gain-
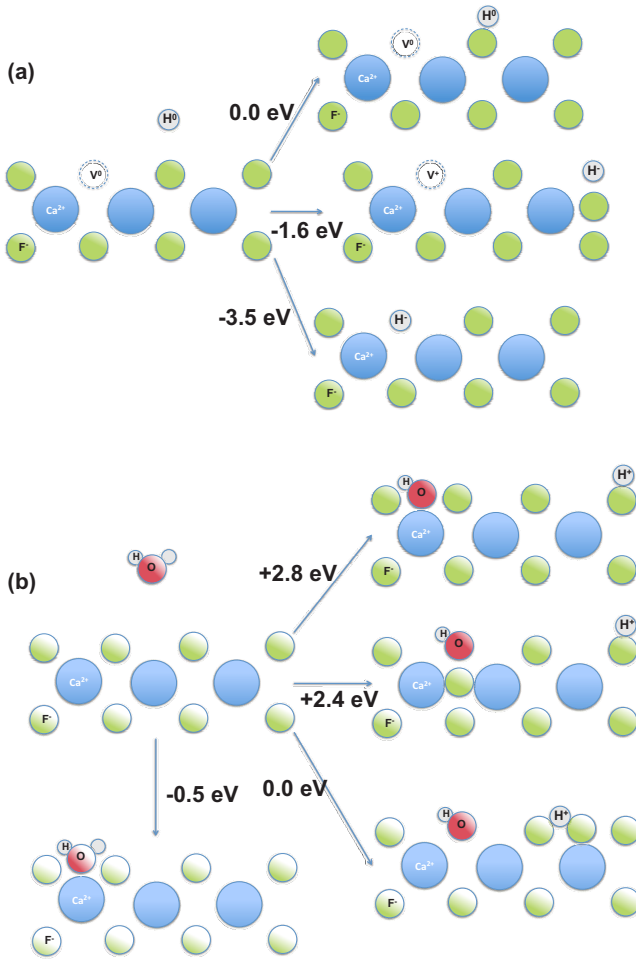
FIG. 7. (Color online) Schematic diagrams showing the different possible reactions and energies for (a) a hydrogen atom adsorbing near a neutral vacancy in the surface, and (b) a water molecule adsorbing onto the ideal surface.

ing about 3.5 eV [see Fig. 7(a)]. At anion and cation sites surrounding the vacancy, hydrogen will immediately return to the vacancy, but at next-nearest anion sites it will undergo displacement process (i), creating its own vacancy to adsorb in [see Fig. 7(a)]. Remembering that hydrogen gains no energy by adsorbing at an anion on the ideal surface, Table X shows that it now gains about 1.6 eV. This is because hydrogen strips the vacancy of its electron, forming H_s^- in the vacancy, a good match for the displaced F^-, and leaving the original vacancy as a V_s^+.

Without the source of this additional electron, i.e., adsorbing near to a charged vacancy V_s^+, the hydrogen forms a proton by donating an electron to the V_s^+, forming V_s^0, and just strongly bonds to a surface F^- ion. The migration barrier between the ground state of hydrogen at a V_s^0 site and this new site is 2.2 eV, suggesting that this state will not exist without external influence.

We have also discovered two other possible reaction paths for dissociation of water at the ideal surface. Firstly, following displacement mechanism (i), the hydroxyl group can displace an F^- ion into a subsurface interstitial site, exposing a vacancy site to adsorb to [see Fig. 7(b)]. This reduces the

adsorption energy (+2.4 eV) by 0.4 eV compared to conventional dissociative adsorption (+2.8 eV), but is still far less favorable than molecular adsorption (−0.5 eV). A further possible reaction route is given by displacement mechanism (ii), whereby in the process of adsorption, water displaces a fluorine ion into an adatom site. During the dissociation process at this new site [see Fig. 7(b)], the dissociated single hydrogen gains a large amount of energy (5.82 eV) by binding to the fluorine adatom, which almost returns the cost of forming the adatom and dissociating the water molecule. The final adsorption energy (0.0 eV) is only 0.5 eV higher than molecular adsorption on the ideal surface, and is almost 3 eV more favorable than conventional dissociation.

IV. DISCUSSION

In this work we have considered the formation of vacancy and interstitial defects in the bulk and at surfaces of CaF_2, SrF_2, and BaF_2, and then explored the adsorption of hydrogen and water on the ideal and defective (111) surfaces. The calculations show that the creation of a neutral vacancy at the surface results in the localization of an electron at the vacancy, forming an F-center defect—as in many other insulators.[13] The barrier for diffusion of this vacancy is smaller than that for bulk vacancies, but it will not be mobile at room temperature. Formation of V_s^0 in the surface layer is favored over the subsurface site. However, formation energies of V_s^+ at the subsurface site are either lower or similar to these at surface site. We show that the barrier for the interchange of the V_s^+ vacancy between the surface and subsurface sites is so small that it will diffuse between them at room temperature (and perhaps migrate across the surface or into the bulk). Both neutral and charged fluorine species adsorbed at the surface as adatoms should be extremely mobile at room temperature.

It is interesting to compare the calculated properties of the vacancies and interstitials with experimental AFM images of the surface.[31,32,36,37] In general, the surfaces are cleaved in UHV before scanning, and it is difficult to imagine that such a destructive process leaves a pristine surface. Indeed, one must assume there is a significant concentration of intrinsic defects at or near the surface. However, the surfaces appear very *clean* in AFM images at the room temperature immediately after cleavage. Adatoms would be too mobile to be visible, and the ease of hopping between surface and subsurface sites, and the migration it facilitates, means that V_s^+ will also be invisible to AFM, if present. This leaves only V_s^0 sites as stable, intrinsic defects at the surface. As discussed in detail, the electron localized at V_s^0 sites matches the removed F^- ion so well that the surrounding cations only relax outward by less than 1%. Since contrast in AFM of ionic surfaces is dominated by electrostatics,[29] this may mean it will appear equivalent to an F^- ion in images, and hence be invisible. However, tip-induced displacements, critical in understanding AFM contrast on CaF_2 at usual scanning ranges,[32] are likely to be very different for an F center compared to a lattice ion and result in different forces.[68,69] Another explanation could be that the density of defects at the surface is so low that the experimental scanning area does not contain any.

Our results show that water will weakly adsorb to the ideal surface, but would prefer to adsorb at vacancies—although the difference in energy is only a few tenths of an eV. Dissociation of water is highly unfavorable on all three ideal surfaces, and remains unfavorable even at neutral and charged vacancy sites in the surface. The only exception to this is a possible route to the dissociated state on CaF_2, where adsorption in the dissociated state is only around 0.2 eV lower in energy at V_s^0 and the barrier to dissociation is about 0.5 eV. This suggests that OH species could exist on the surface if there is a significant density of neutral vacancies present.

Our calculations of the diffusion barriers show that molecular water is extremely mobile on the surface, even when adsorbed at defects, and is only strongly bound in the dissociated state at neutral vacancies in CaF_2. In general, CaF_2 and SrF_2 show similar behavior with respect to water, while adsorption energies and migration barriers for BaF_2 are smaller due to its significantly larger lattice constant. Our results also give some indication of the possible identity of mobile and immobile defects seen in high resolution AFM manipulation experiments on the water dosed CaF_2 (111) surface.[37] It is likely that vacancies play a role in determining the state of water on the surface, since it is so mobile without them. However, without a detailed study of the manipulation process of all these defect complexes, including the role of tip-induced effects, it is impossible to make a comprehensive explanation or exclude the role of other impurities in the measurements.

More generally, our comprehensive treatment of defects and adsorbates provides insight into the differences between the three alkali-earth materials, but also offers information on how water adsorbs, reacts and diffuses relevant to all insulating surfaces. The presence of surface and subsurface defects in insulating oxide surfaces has recently been highlighted,[60,70,71] and it will be critical to study how these affect the interaction of water with the surface.

[1] D. J. Müeller and Y. F. Dufrêne, Nat. Nanotechnol. **3**, 261 (2008).

[2] M. A. Henderson, Surf. Sci. Rep. **46**, 1 (2002).

[3] K. H. Rao, J. M. Cases, P. de Donato, and K. S. E. Forssberg, J. Colloid Interface Sci. **145**, 314 (1991).

[4] M. L. Free and J. D. Miller, Langmuir **13**, 4377 (1997).

[5] L. Pasquali, S. M. Suturin, V. P. Ulin, N. S. Sokolov, G. Selvaggi, A. Giglia, N. Mahne, M. Pedio, and S. Nannarone, Phys. Rev. B **72**, 045448 (2005).

[6] L. Pasquali, S. M. Suturin, A. K. Kaveev, V. P. Ulin, N. S. Sokolov, B. P. Doyle, and S. Nannarone, Phys. Rev. B **75**, 075403 (2007).

[7] C. R. A. Catlow and M. J. Norgett, J. Phys. C **6**, 1325 (1973).

[8] R. T. PooleJ. Szajman, R. C. G. Leckey, J. G. Jenkin, and J. Liesegang, Phys. Rev. B **12**, 5872 (1975).

[9] P. W. M. Jacobs and S. H. Ong, J. Phys. Colloq. **37**, C7 (1976).

[10] J. Atobe, J. Chem. Phys. **71**, 2588 (1979).

[11] J. Oberschmidt and D. Lazarus, Phys. Rev. B **21**, 5823 (1980).

[12] S. Parker, K. Song, C. Catlow, and A. Stoneham, J. Phys. C **14**, 4009 (1981).

[13] W. Hayes and A. M. Stoneham, *Defects and Defect Processes in Non-Metallic Solids* (Wiley, New York, 1985).

[14] J. H. Harding, Phys. Rev. B **32**, 6861 (1985).

[15] A. Jockisch, U. Schröder, F. W. de Wette, and W. Kress, J. Phys.: Condens. Matter **5**, 5401 (1993).

[16] M. Riechling, M. Huisinga, D. Ochs, and V. Kempter, Surf. Sci. **402-404**, 145 (1998).

[17] M. Huisinga, N. Bouchaala, R. Bennewitz, E. Kotomin, M. Reichling, V. Kuzovkov, and W. von Niessen, Nucl. Instrum. Methods Phys. Res. B **141**, 79 (1998).

[18] A. V. Puchina, V. E. Puchin, M. Huisinga, R. Bennewitz, and M. Reichling, Surf. Sci. **402-404**, 687 (1998).

[19] V. Puchin, A. Puchina, M. Huisinga, and M. Reichling, J. Phys.: Condens. Matter **13**, 2081 (2001).

[20] J. Vogt, J. Henning, and H. Weiss, Surf. Sci. **578**, 57 (2005).

[21] N. H. de Leeuw and T. G. Cooper, J. Mater. Chem. **13**, 93 (2003).

[22] C. R. A. Catlow, J. Phys. Chem. Solids **38**, 1131 (1977).

[23] Y. Wu, J. T. Mayer, E. Garfunkel, and T. E. Madey, Langmuir **10**, 1482 (1994).

[24] G. Jordan and W. Rammensee, Surf. Sci. **371**, 371 (1997).

[25] K. A. Becraft and G. L. Richmond, Langmuir **17**, 7721 (2001).

[26] *Noncontact Atomic Force Microscopy*, edited by S. Morita, R. Wiesendanger, and E. Meyer (Springer, Berlin, 2002).

[27] R. García and R. Pérez, Surf. Sci. Rep. **47**, 197 (2002).

[28] F. J. Giessibl, Rev. Mod. Phys. **75**, 949 (2003).

[29] W. Hofer, A. S. Foster, and A. L. Shluger, Rev. Mod. Phys. **75**, 1287 (2003).

[30] A. S. Foster, C. Barth, A. L. Shluger, and M. Reichling, Phys. Rev. Lett. **86**, 2373 (2001).

[31] C. Barth, A. S. Foster, M. Reichling, and A. L. Shluger, J. Phys.: Condens. Matter **13**, 2061 (2001).

[32] A. S. Foster, C. Barth, A. L. Shluger, R. M. Nieminen, and M. Reichling, Phys. Rev. B **66**, 235417 (2002).

[33] R. Hoffmann, C. Barth, A. S. Foster, A. L. Shluger, H. J. Hug, H. J. Güntherodt, R. M. Nieminen, and M. Reichling, J. Am. Chem. Soc. **127**, 17863 (2005).

[34] R. Bennewitz, M. Reichling, and E. Matthias, Surf. Sci. **387**, 69 (1997).

[35] M. Reichling and C. Barth, Phys. Rev. Lett. **83**, 768 (1999).

[36] S. Fujii and M. Fujihira, Jpn. J. Appl. Phys. **45**, 1986 (2006).

[37] S. Hirth, F. Ostendorf, and M. Reichling, Nanotechnology **17**, S148 (2006).

[38] G. Kresse and J. Furthmüller, Comput. Mater. Sci. **6**, 15 (1996).

[39] G. Kresse and J. Furthmüller, Phys. Rev. B **54**, 11169 (1996).

[40] J. P. Perdew, K. Burke, and M. Ernzerhof, Phys. Rev. Lett. **77**, 3865 (1996).

[41] P. E. Blöchl, Phys. Rev. B **50**, 17953 (1994).

[42] G. Kresse and D. Joubert, Phys. Rev. B **59**, 1758 (1999).

[43] H. J. Monkhorst and J. D. Pack, Phys. Rev. B **13**, 5188 (1976).

[44] G. Rubloff, Phys. Rev. B **5**, 662 (1972).

[45] S. Kuemmel and L. Kronik, Rev. Mod. Phys. **80**, 3 (2008).

[46] G. Henkelman, B. Uberuaga, and H. Jónsson, J. Chem. Phys. **113**, 9901 (2000).

[47] C. V. de Walle and J. Neugebauer, J. Appl. Phys. **95**, 3851 (2004).

[48] *Handbook of Chemistry and Physics*, 84th ed., edited by D. R. Lide (CRC Press, Boca Raton, 2003).

[49] G. Makov and M. C. Payne, Phys. Rev. B **51**, 4014 (1995).

[50] L. N. Kantorovich, Phys. Rev. B **60**, 15476 (1999).

[51] K.-D. Li, H. Y. Xiao, and L. M. Wang, Nucl. Instrum. Methods Phys. Res. B **266**, 2698 (2008).

[52] C. Leung, G. Brunet, and K. Song, J. Phys. C **18**, 4459 (1985).

[53] A. B. Lidiard, *Handbuch der Physik XX* (Springer-Verlag, Berlin, 1957).

[54] A. S. Foster, A. L. Shluger, and R. M. Nieminen, Phys. Rev. Lett. **89**, 225901 (2002).

[55] Y. Ma and M. Rohlfing, Phys. Rev. B **77**, 115118 (2008).

[56] D. Munoz Ramo, J. L. Gavartin, A. L. Shluger, and G. Bersuker, Phys. Rev. B **75**, 205336 (2007).

[57] A. L. Shluger, V. E. Puchin, T. Suzuki, K. Tanimura, and N. Itoh,

[58] B. Li, A. Michaelides, and M. Scheffler, Phys. Rev. Lett. **97**, 046802 (2006).

[59] R. Jia, H. Shi, and G. Borstel, Comput. Mater. Sci. **43**, 980 (2008).

[60] M. V. Ganduglia-Pirovano, J. L. F. Da Silva, and J. Sauer, Phys. Rev. Lett. **102**, 026101 (2009).

[61] M. B. Watkins, A. S. Foster, and A. L. Shluger, J. Phys. Chem. C **111**, 15337 (2007).

[62] M. Watkins, T. Trevethan, A. L. Shluger, and L. N. Kantorovich, Phys. Rev. B **76**, 245421 (2007).

[63] S. Wendt, J. Matthiesen, R. Schaub, E. K. Vestergaard, E. Laegsgaard, F. Besenbacher, and B. Hammer, Phys. Rev. Lett. **96**, 066107 (2006).

[64] P. Maksyutenko, T. R. Rizzo, and O. V. Boyarkin, J. Chem. Phys. **125**, 181101 (2006).

[65] L. Branscomb, Phys. Rev. **148**, 11 (1966).

[66] J. Ortiz, J. Chem. Phys. **86**, 308 (1987).

[67] T. Yoshida, G. Miyako, N. Jiang, and D. M. Schrader, Phys. Rev. A **54**, 964 (1996).

[68] A. S. Foster, O. H. Pakarinen, J. M. Airaksinen, J. D. Gale, and R. M. Nieminen, Phys. Rev. B **68**, 195410 (2003).

[69] T. Trevethan and A. L. Shluger, Nanotechnology **20**, 264019 (2009).

[70] S. Wendt *et al.*, Science **320**, 1755 (2008).

[71] G. H. Enevoldsen, H. P. Pinto, A. S. Foster, M. C. R. Jensen, W. A. Hofer, B. Hammer, J. V. Lauritsen, and F. Besenbacher, Phys. Rev. Lett. **102**, 136103 (2009).

[72] W. Humphrey, A. Dalke, and K. Schulten, J. Mol. Graphics **14**, 33 (1996).